Enhancement of Fiber Orientation Distribution Reconstruction in Diffusion-Weighted Imaging by Single Channel Blind Source Separation

Min Jing*, T. Martin McGinnity, *Senior Member, IEEE*, Sonya Coleman, *Member, IEEE*, Huaizhong Zhang, *Member, IEEE*, Armin Fuchs, and J. A. Scott Kelso

***Abstract*—In diffusion-weighted imaging (DWI), reliable fiber tracking results rely on the accurate reconstruction of the fiber orientation distribution function (fODF) in each individual voxel. For high angular resolution diffusion imaging (HARDI), deconvolution-based approaches can reconstruct the complex fODF and have advantages in terms of computational efficiency and no need to estimate the number of distinct fiber populations. However, HARDI-based methods usually require relatively high b-values and a large number of gradient directions to produce good results. Such requirements are not always easy to meet in common clinical studies due to limitations in MRI facilities. Moreover, most of these approaches are sensitive to noise. In this study, we propose a new framework to enhance the performance of the spherical deconvolution (SD) approach in low angular resolution DWI by employing a single channel blind source separation (BSS) technique to decompose the fODF initially estimated by SD such that the desired fODF can be extracted from the noisy background. The results based on numerical simulations and two phantom datasets demonstrate that the proposed method achieves better performance than SD in terms of robustness to noise and variation in b-values. In addition, the results show that the proposed method has the potential to be applied to low angular resolution DWI which is commonly used in clinical studies.**

***Index Terms*—Diffusion-weighted imaging, fODF reconstruction, single channel blind source separation, spherical deconvolution.**

I. Introduction

To date, diffusion-weighted imaging (DWI) is a noninvasive tool available to reveal the neural architecture of human brain white matter. The signal observed from one voxel in diffusion-weighted MRI is related to the displacement distribution of the water molecules in this voxel. By analysing and quantifying diffusivity, valuable information about the inner fiber structure of the brain can be obtained. Advances in DWI techniques have shown great potential in the study of brain white matter related diseases such as depression [3], traumatic brain injury [4], [5], and Alzheimer's disease [6].

In the early proposed diffusion tensor imaging (DTI) model [1], the orientation and strength of anisotropic diffusion were derived based upon eigenvectors and eigenvalues of the estimated diffusion tensor profile. It was found that the early DTI model is inadequate to characterize the complexity of tissue structure such as multiple fibers within a voxel due to its Gaussian assumption. The newly developed technique high angular resolution diffusion imaging (HARDI) [7] has shown capability to reconstruct complex fiber orientation information within a voxel by applying advanced reconstruction techniques such as diffusion spectrum imaging (DSI) [9], q-ball imaging (QBI) [8], persistent angular structure (PAS) [10], diffusion orientation transform (DOT) [11], and spherical deconvolution (SD) [12]. The inner fiber structure, which presents the connection between voxels, can be delineated by fiber tractography based upon the reliable fiber orientation distribution obtained from each individual voxel. An intensive review of reconstruction methods can be found in [13].

In general, deconvolution-based reconstruction methods have advantages due to not having to specify the number of distinct fiber populations, being able to provide the actual fiber orientation and computational efficiency. In the deconvolution model, the measured diffusion signal is considered as the convolution over the unit sphere of a response function (kernel) with the fODF. Different deconvolution-based methods have been developed for fODF reconstruction [12], [23]–[25], [27], [28]. The differences between these methods mainly reside in terms of construction of the response function, the strategies to deal

Manuscript received May 26, 2011; revised August 19, 2011; accepted September 14, 2011. Date of publication October 19, 2011; date of current version January 20, 2012. This work was supported by the Northern Ireland Department for Education and Learning "Strengthening the All-island Research Base" project. The works of A. Fuchs and J. A. S. Kelso were supported by NIMH Grant MH080838. The work of S. Coleman was supported in part by EPSRC award EP/C006283/11, the Nuffield Foundation, and The Leverhulme Trust. *Asterisk indicates corresponding author.*

*M. Jing is with the Intelligent Systems Research Centre, School of Computing and Intelligent Systems, University of Ulster, BT48 7JL U.K. (e-mail: m.jing@ulster.ac.uk).

T. M. McGinnity, S. Coleman, and H. Zhang are with the Intelligent Systems Research Centre, School of Computing and Intelligent Systems, University of Ulster, BT48 7JL U.K. (e-mail: tm.mcginnity@ulster.ac.uk; sa.coleman@ulster.ac.uk; h.zhang@ulster.ac.uk).

A. Fuchs is with the Human Brain and Behavior Laboratory (HBBL), Center for Complex Systems and Brain Sciences, Florida Atlantic University, USA (e-mail: fuchs@ccs.fau.edu).

J. A. S. Kelso is with with the Intelligent Systems Research Centre, School of Computing and Intelligent Systems, University of Ulster, BT48 7JL U.K., and with the Human Brain and Behavior Laboratory (HBBL), Center for Complex Systems and Brain Sciences, Florida Atlantic University, USA (e-mail: kelso@ccs.fau.edu).

Digital Object Identifier 10.1109/TBME.2011.2172793

with negative values in the reconstructed fODF and to improve the angular resolution of fODF. A response function can be derived directly from real data based on averaging the DWI signals from hundreds of voxels which have high fractional anisotropy (FA) [12]; or it can be formed based on a single fiber response in which the principal diffusiveness is uniquely defined [25]. Another problem in deconvolution-based methods is the presence of meaningless negative values in the reconstructed fODF which can be, due to truncation of the harmonic series, using inappropriate response functions and noise [12]. To deal with this problem, a constraint can be imposed by using the Richardson-Lucy iterative algorithm [28], Tikhonov regularization [24] or non-negative least squares optimization [27]. Alternatively, in [15] the effect of negative values is reduced by using a lower order spherical harmonic (SH) series followed by deconvolution as a sharpening process to increase the angular resolution of the fODF.

Like most HARDI-based methods, deconvolution methods are sensitive to noise. Noise can cause negative values and spurious peaks in the fODF, and affect the accuracy in final fODF results. A common way to deal with noise is to apply a low pass filter to remove the high frequency components. However, filtering can also remove some useful information since the attenuation process in filtering always removes parts of the signal, which can reduce the angular resolution and result in a smoothed fODF. In this study we propose a novel approach, in which the fODF can be extracted from noisy data by employing the blind source separation (BSS) technique, thereby the performance of fODF reconstruction can be enhanced without compromising angular resolution in the final fODF.

As an effective BSS technique, independent component analysis (ICA) has been successfully used in decomposition of EEG and functional MRI (fMRI) signals [16], [17], in which the desired source can be extracted as an independent component (IC) from a noisy background. The advantages of ICA have not been fully exploited in DWI so far. Only a few papers have addressed this area. In [18], ICA was applied to raw DWI images under the assumption that the data are a linear combination of spatially independent components. The results demonstrated that ICA can separate noise, eddy current effects and some fiber tracts from image data. In [19], a joint ICA was used to decompose the FA map and fMRI data in order to investigate inner brain connectivity. In [20], the orientation of two crossing fibers was estimated by decomposing the data from multiple voxels based on the assumption that neighbouring voxels contain the same fiber tracts. In [21], ICA was used to segment the thalamus by decomposition of fiber tracts obtained from probabilistic tractography. In our recent study [29], ICA has been applied to a mixture of diffusion ODF (dODF) estimated by analytical QBI (AQBI) [31] based on the signal from one voxel only. (The relationship between dODF and fODF is still an open question, it is usually considered that dODF is a "blurred version" of fODF [14].) By dividing the gradient directions into a number of groups, a mixture was formed by dODFs estimated from each group, then ICA was applied to separate the desired dODF from the mixture. The results show that ICA can not only extract the desired dODF effectively, but also can achieve better performance than the AQBI solution when the data have a low signal-to-noise-ratio (SNR).

There are two objectives of this study. The first objective is to develop an effective framework in which the advantages of ICA can be incorporated into fODF reconstruction based on the signal from a single voxel only. The second objective is to explore the potential to apply such a framework to DWI data acquired with low angular resolution, since this type of DWI data are easily acquired and commonly used in current clinical studies. The HARDI based methods can solve the problem of complex fiber orientation reconstruction; however they require data to be acquired under high angular resolution, high spatial resolution, and relatively high b-values. Such requirements are not always easy to meet in practice due to limitations in MRI facilities. For example, in most clinical studies, DWI data are usually collected with b-value less than or equal to $1000\,\mathrm{s/mm^2}$ and the number of gradient directions is less than 25. Therefore, the HARDI-based reconstruction methods have not been widely applied in clinical studies. To date, eigenvalue-based quantification, such as FA, is still most commonly used in clinical studies for neurological disease even though the limitations in the DT model are well known.

In this paper, we present a novel framework in which a single channel ICA (sICA) is applied to a fODF initially estimated from SD in low angular resolution DWI data. The initial estimation of fODF is considered as a mixed signal containing noise, bias/artifacts and the desired fODF to be separated from the mixture by sICA. The results from numerical simulations, phantom datasets and in vivo data demonstrate that the proposed method can not only successfully extract the desired fODF and improve the reconstruction performance in terms of robustness to noise and variation in b-values, but also has the potential to be applied to low angular resolution DWI data used for clinical studies.

The paper is organized as follows: In Section II, background on the DTI model and SD method is provided. In Section III, the proposed method and sICA model are explained in detail. Experimental results are presented in Section IV. The proposed method is evaluated by both synthetic data, phantom data and *in vivo* data, and the results are compared with the SD method and AQBI. Discussion and conclusion are given in Section V.

II. Background

A. Diffusion Tensor Imaging

In the diffusion tensor model [2], for a given voxel with magnetic gradient direction $\mathbf{g}_i$, the diffusion signal $\mathbf{s}$ measured based on this direction can be expressed as

$$\mathbf{s}(\mathbf{g}_i) = \mathbf{s}_0 \exp(-b\mathbf{g}_i^T \mathbf{D}\mathbf{g}_i) \tag{1}$$

where $\mathbf{s}_0$ denotes the DWI signal with no gradient applied. The gradient direction is given as $\mathbf{g}_i = [\sin(\theta_i)\cos(\phi_i), \sin(\theta_i)\sin(\phi_i), \cos(\theta_i)]^T$, where θ and ϕ are the elevation and azimuthal angle in the spherical coordinates, respectively ($\theta \in [0, \pi], \phi \in [0, 2\pi)$). T denotes the transpose operator. $\mathbf{D}$ is a diffusion profile to describe the molecular mobility along each direction, which can be represented by

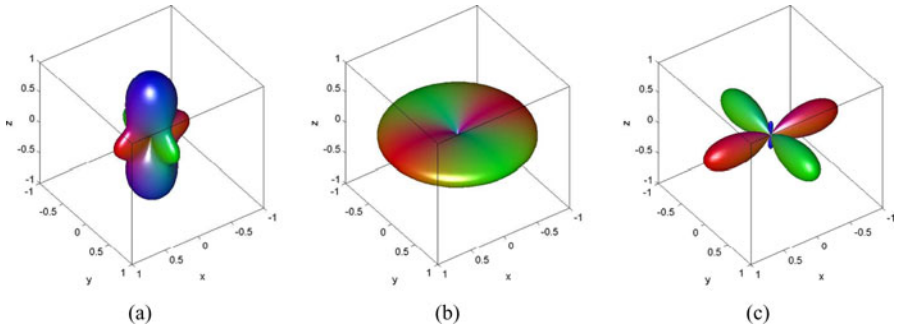

Fig. 1. Illustration of fODF reconstruction by the SD method: (a) Synthetic DWI signal generated from two crossing fibers, (b) response function generated from a single fiber with fiber orientation along with z-axis, and (c) reconstructed fODF by the SD method which shows two crossing fibers.

eigenvalues estimated from the diffusion profile. A b-value is used to characterize the gradient pulses in MRI sequences, which is based on the strength and duration of the gradient pulse, and the time interval between the onset of the two gradient pulses. The b-value plays an important role in DWI data acquisition. If the b-value is too small, the signal can be too smooth to have enough contrast. A higher b-value can increase the contrast, however, it also increases the acquisition time and the noise level in the data. In clinical studies, the selection of a b-value needs to take these factors into account.

B. Reconstruction of fODF by Spherical Deconvolution

In [12], a spherical deconvolution (SD) model was proposed for fODF reconstruction by adopting the approach in [22]. Based on the SD model, the measured diffusion signal is considered as the convolution over the unit sphere of a response function with a fiber orientation density function. The response function is defined as an axially symmetric function with the fiber orientation aligned with the z-axis. By employing the technique of spherical harmonic transform (SHT), a Fourier analysis tool in spherical space, the spherical deconvolution can be simplified to a matrix multiplication since the convolution of two functions is equivalent to matrix multiplication in Fourier space. After SHT, the deconvolution problem can be expressed as

$$\bar{\mathbf{s}} = \bar{\mathbf{H}}\bar{\mathbf{f}} \tag{2}$$

where $\bar{\mathbf{s}}$ is an $L \times 1$ vector representing the spherical harmonic (SH) coefficients of the DWI signal $\mathbf{s}$, L is the length of the SH series and depends on the order of spherical harmonics. $\bar{\mathbf{f}}$ is also an $L \times 1$ vector denoting the SH coefficients of the fODF. $\bar{\mathbf{H}}$ is an $L \times L$ matrix representing the SH of the response function, which is also referred to as rotational harmonic coefficients in [22]. An illustration of fODF reconstruction by the SD method is given in Fig. 1. More details about SHT can be found in [22], [31].

As in all inverse problems, the SD solution is ill-posed and sensitive to noise. The level of sensitivity to noise increases with the order of the SH. As mentioned in [12], the noise is also a primary factor causing physically meaningless negative values in the fODF results. Apart from these, SD relies on the estimation of a response function, which is assumed to be constant throughout the brain. Such assumptions are not fulfilled in regions where the white matter fibers have significantly different diffusion characteristics, though this may only affect the volume fraction of fiber populations but not the orientation itself [12].

III. Method

In this study, we aim to develop a framework in which ICA can be utilized in DWI signals obtained within a single voxel so that the performance of fODF reconstruction in a low angular resolution DWI can be enhanced. To date, only limited studies have been reported in applying ICA to DWI data analysis, in which ICA was used to decompose FA maps [19], DWI images [18], fiber tracts [21], DWI signals from multiple voxels [20] and a single voxel [29]. There are two problems when applying ICA to DWI signals obtained from a single voxel: first, ICA is usually used for multichannel data decomposition, but the DWI signal from one voxel is a vector with length equal to the number of gradient directions, so conventional ICA cannot be applied directly; second, the direction corresponding to the maximum of a DWI signal does not lie in the same plane as the fODF (as shown in Fig. 1) due to rotation and summation in the spherical system. Therefore, applying ICA to the DWI signal can only produce the components of a DWI signal but not the components of the fODF. Here we propose a novel framework in which a single channel ICA is employed to decompose an fODF initially estimated by SD. This initial estimation of fODF can be considered as a signal mixed with noise, artifacts, and the desired "true" fODF to be extracted by the separation process of sICA.

A. Single Channel ICA Model

ICA decomposes multichannel data into statistically independent components. Generally, it assumes that the source components are statistically independent, the number of input channels is greater or equal to the number of sources, and at most only one source can have a Gaussian distribution. When there is only one channel recording available, the decomposition process can be performed by a single channel ICA (sICA) model. An early approach for the sICA problem was related to "sparse coding" [34] and sparse decomposition [35]. The sICA has been applied to the decomposition of a single channel acoustic signal [36], EEG [37], [38], and abdominal phonogram [39].

In the sICA model, single channel data with length L is considered as a linear superposition of a number of basis functions with their corresponding weight coefficients. By truncating the data with a window of length N ($N < L$) and stacking successive truncated data $\mathbf{x}$, a data matrix can be constructed as

$$\begin{pmatrix} x(k) & x(k+1) & \cdots & x(L-N+1) \\ x(k+1) & x(k+2) & \cdots & x(L-N+2) \\ \vdots & \vdots & \vdots & \vdots \\ x(k+N-1) & x(k+N) & \cdots & x(L) \end{pmatrix}. \quad (3)$$

The sICA model can then be expressed as

$$\mathbf{x} = \mathbf{A}\mathbf{v} \quad (4)$$

where $\mathbf{x}$ is an N-dimensional column vector represented as $\mathbf{x}(k) = [x(k), x(k+1), \ldots, x(k+N-1)]^T$. $\mathbf{A}$ is an $N \times M$ matrix with M basis functions represented by its column vectors. $\mathbf{v}$ is the weight coefficient corresponding to the basis function. (Note that noise is considered as a source signal in the model.) The purpose of decomposition is to find a linear transformation to give an estimation of $\mathbf{v}$, denoted as $\mathbf{y} = \mathbf{W}\mathbf{x}$, by which the elements of the coefficient $\mathbf{y}$ are statistically independent, and $\mathbf{W} = \mathbf{A}^{\dagger}$ is the pseudoinverse of $\mathbf{A}$.

In this study, the inputs for sICA are the SH coefficients of the fODF initially estimated by SD (2) and we want to extract the desired fODF from noise by learning of the basis functions by sICA. The reason for decomposing the SH of the fODF rather than the fODF itself is that it has been found that sICA can only result in successful separation when the components have a disjoined power spectrum [37]. In our simulation, it turns out to be true for the SH of noise and the SH of fODF. (For decomposition of a signal with spectrally overlapping sources refer to [38], which applies the empirical mode decomposition (EMD) to decompose a given signal into spectrally independent modes followed by ICA.) It should be noted that the performance of sICA is affected by the window length for data truncation. In [37], the window length was chosen empirically. In [39], the data matrix was considered as an embedding matrix by taking time delay and embedding dimension into account. In this study, the window length is determined based on results from numerical simulations.

B. Learning Basis Function

After construction of a data matrix, the basis functions can be learned by standard ICA. Selection of the separation algorithm depends on an assumption about the distribution of the data sources, which is still unknown for DWI signals. However, Infomax (information-maximization) has been applied in [20] and our previous work [29], therefore, Infomax is used in this study. Infomax is based on information theory by maximizing the output entropy, which is closely related to the maximum likelihood (ML) estimation. An efficient way to maximize the log-likelihood is to apply the natural gradient learning method, which is given as [33]

$$\triangle \mathbf{W} \propto \frac{\partial H(\mathbf{y}, \mathbf{W})}{\partial \mathbf{W}} \mathbf{W}^T \mathbf{W} = [\mathbf{I} - \varphi(\mathbf{y})\mathbf{y}^T]\mathbf{W} \quad (5)$$

where $\mathbf{I}$ is the identity matrix and $\varphi(\mathbf{y})$ is the nonlinear function. The adaptive learning rule can be written as

$$\mathbf{W}(n+1) = \mathbf{W}(n) - \eta(n)[\mathbf{I} - \varphi(\mathbf{y}(n))\mathbf{y}(n)^T]\mathbf{W}(n) \quad (6)$$

where n is the iteration number and $\eta(n)$ is the learning rate. After learning the basis functions, the ICs can be recovered by the process explained in the following section.

C. Reconstruction of ICs

To reconstruct the ICs, we first project each component back to its original signal space, which can be performed by multiplying the ith column vector of the inverse of the unmixing matrix by the corresponding IC

$$\mathbf{X}_p(i) = [\mathbf{W}^{\dagger}]_i \mathbf{y}_i \quad (7)$$

where $\mathbf{X}_p(i)$ denotes the back projection of the ith IC in the original data matrix (3). The ith IC with the original length can be recovered from $\mathbf{X}_p(i)$ by diagonal averaging [41] as applied in [39], [42], which is expressed as

$$IC = \begin{cases} \dfrac{1}{j+1} \displaystyle\sum_{i=1}^{j+1} \mathbf{X}_{p(i,j-i+2)} & 0 \le j < R-1 \quad (8a) \\ \dfrac{1}{R} \displaystyle\sum_{i=1}^{R} \mathbf{X}_{p(i,j-i+2)} & R-1 \le j < C \quad (8b) \\ \dfrac{1}{L-j} \displaystyle\sum_{i=j-C+2}^{L-C+1} \mathbf{X}_{p(i,j-i+2)} & C \le j < L \quad (8c) \end{cases}$$

where $R = \min(N, L-N+1)$, $C = \max(N, L-N+1)$ and $L = R + C - 1$. Note that the reconstructed ICs are the SH coefficients, the final fODF can be obtained by back projection of the SH coefficients on the sphere.

IV. Results

This section contains results from numerical simulations, phantom data and *in vivo* data. In all parts, the SH order was set to 4 because our main focus was on the DWI data with low angular resolution. For 25 directions, only order-4 can be applied. For SD method, using order-4 can also reduce the effect of noise. The number of ICs in sICA was set to 2. It was based on the assumption that the fODFs and noise are statistically independent, and we only wish to obtain these two ICs from the output. The IC with greater energy was selected as the desired fODF. Further explanation about the parameter settings is given in the discussion section.

A. Numerical Simulation

The numerical simulations include three parts: 1) illustration of separation by sICA, 2) performance under various b-values, and 3) robustness to noise. Three methods, unfiltered SD (UFSD), filtered SD (FSD), and sICA, were applied. The filtering was performed by multiplying the lth order SH with an attenuation factor β, the smaller the factor, the greater the attenuation. In [12], $\beta = [1, 1, 1, 0.8, 0.1]$ was used for an order-8 case. In this study, β was empirically set as [1, 1, 0.67] for order-4.

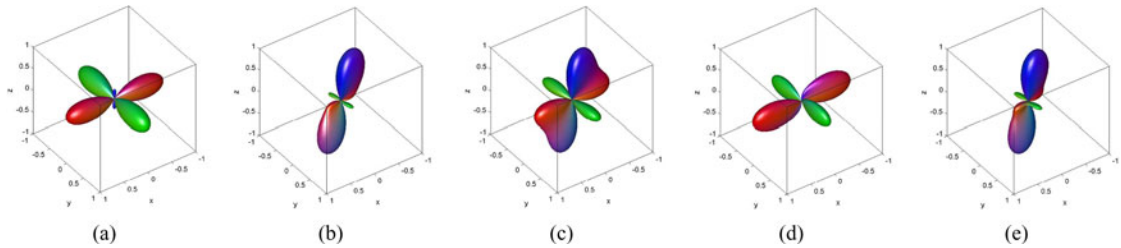

Fig. 2. Illustration of the separation by sICA: (a) Source-1 (fODF), (b) source-2, (c) mixed signal, (d) IC1, and (e) IC2, which shows that the fODF is successfully separated from the mixed signal.

To evaluate the performance, the results are compared with a "ground truth." Here, the fODF estimated by SD from the noise-free DWI is considered as the "ground truth." A similar approach for evaluation of reconstruction performance has been used in [7], [8], [30], [31]. Two metrics are used: correlation coefficient and mean square error (MSE). The correlation coefficient compares the closeness between two random variables, which is commonly used in ICA-related approaches for results comparison. It is defined as a normalized version of covariance [40]

$$cor(\mathbf{y}, \hat{\mathbf{y}}) = \frac{cov(\mathbf{y}, \hat{\mathbf{y}})}{\sigma_{\mathbf{y}} \sigma_{\hat{\mathbf{y}}}} \tag{9}$$

where $\mathbf{y}$ represents the SH coefficients estimated by SD from noise-free data, $\hat{\mathbf{y}}$ is the estimated SH of fODF, σ denotes the standard deviation, and $cov(\cdot)$ is the lag zero covariance. MSE has been used for ODF shape comparison [7], [8], [30], [31]. The "shape" of ODF is a back projection of the SH coefficients onto a unit sphere, which is a real-valued function. As used in [30], [31], MSE is calculated by

$$mse(\mathbf{f}, \hat{\mathbf{f}}) = \frac{1}{K} \sum_{i=1}^{K} \|f_i - \hat{f}_i\|^2 \tag{10}$$

where $\mathbf{f}$ represents the "true" fODF, $\hat{\mathbf{f}}$ is the estimated fODF, and K is the length of $\mathbf{f}$.

1) Synthetic Diffusion Data Generation: The synthetic DWI data were generated based on the multitensor model as in [32]. The model assumes that the single fiber response can be described by a Gaussian (rank-2 tensor) and the DWI signal can be approximated by the sum of signals generated from the directionally distinct fiber populations. In this study, only two fiber populations were generated, with a separating angle of 90° and the weight factor for each fiber population was selected as 0.5. A close approximation of real data was obtained by using the same gradient directions and b-value as in the *in vivo* data collection. The gradient directions were 25 and 55, and the b-value $1000\ \mathrm{s/mm^2}$. Complex Gaussian noise was added to produce a signal with SNR of $1/\sigma$, where σ is the standard deviation of noise. Although there are studies in which noise with a Rician distribution is applied [43], complex Gaussian noise has also been used in the numerical simulation [12], [28], [30], [31]. Here, complex Gaussian noise is applied as we mainly compare our approach with the methods proposed in [12], [31].

2) Illustration of Separation by sICA: To illustrate the performance of the separation process by sICA, two source signals were generated. The first source was the fODF of two fiber populations with crossing angle 90°, the second source was the signal to simulate the noise. The mixed signal was the sum of the two sources. The process of separation is illustrated in Fig. 2, which shows source-1, source-2, mixed signal, IC1, and IC2, respectively. The signals are plotted as spherical functions, in which the amplitudes of functions are directionally colour-coded (red for left-right, green for anterior-posterior, and blue for superior-inferior). It can be seen from Fig. 2 that after performing sICA, the fODF of the crossing fiber is successfully separated from the mixed signal.

3) Performance Under Various b-Values: The selection of an optimal b-value in DWI acquisition is still an ongoing issue. The SNR of DWI signals decreases with increasing b-value; but if the b-value is too small, the signal can be too smooth to have enough contrast. For the AQBI method [31], a low estimation error is observed for b-values of 2,000–6,000 $\mathrm{s/mm^2}$. For the SD method [12], optimal results are observed at a b-value of 3000 $\mathrm{s/mm^2}$ with $\mathrm{SNR} = 30\,\mathrm{dB}$. Here three methods, UFSD, FSD, and sICA, were applied to synthetic data with $\mathrm{SNR} = 10\,\mathrm{dB}$, and directions of 25 and 55. In total 50 noise trials were done and the mean of the correlation and MSE between "ground truth" and each of the three methods were calculated. The results from 25 and 55 directions are given in Figs. 3 and 4, respectively. The number of direction is denoted by Ng.

As expected, the performance from direction $Ng = 55$ is better than $Ng = 25$, indicated by a smaller MSE and higher correlation. In both $Ng = 25$ and $Ng = 55$, it is observed that a small estimation error occurs when the b-value is between 1,000 and 3,000 $\mathrm{s/mm^2}$. For low b-values, the results from FSD do not show apparent improvement compared to UFSD. This is because the SD method is more sensitive to noise for higher SH orders, so filtering does not have much impact for SH of order-4. For high b-values (high noise level), it is noticed that FSD has an MSE higher than UFSD, which indicates the increased error in shape of ODFs due to the smoothing effect of filtering. (The visualization of the smoothing effect is demonstrated in phantom data results.) For all b-values, sICA consistently achieves higher correlation and smaller MSE than UFSD and FSD, which clearly demonstrates the superiority of sICA.

4) Robustness to Noise: The three methods were applied to synthetic data with SNR varied from 5 dB to 55 dB and $\mathrm{b} = 1000\ \mathrm{s/mm^2}$. The 50 noise trials were done and the means of the correlation and MSE were calculated. Results from 25 and 55 directions are given in Figs. 5 and 6, respectively. It can

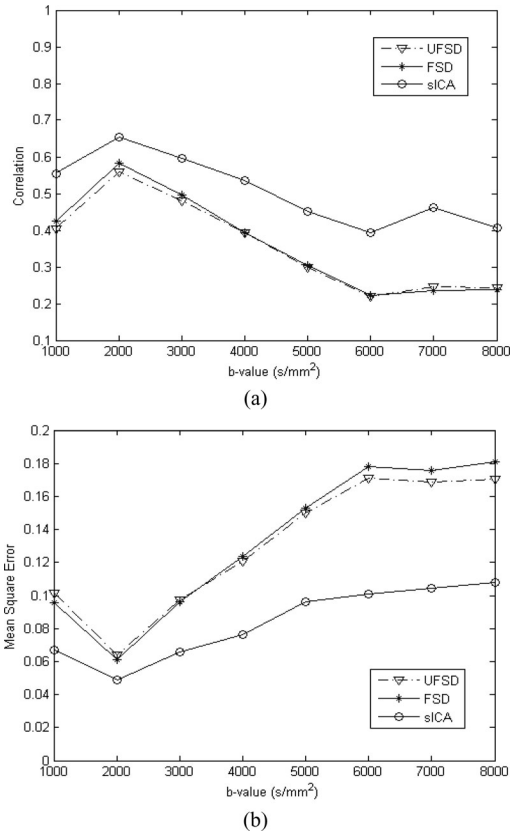

Fig. 3. Comparison of the performance under various b-values, $Ng = 25$. (a) Correlation coefficients, (b) MSE.

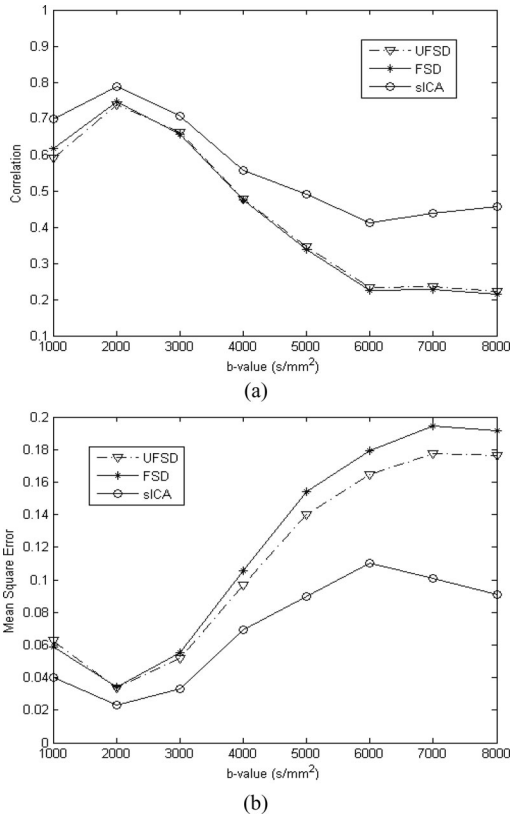

Fig. 4. Comparison of the performance under various b-values, $Ng = 55$. (a) Correlation coefficients, (b) MSE.

be seen that for all methods the performance improves with increasing SNR. For good quality data (high SNR), the results from all methods are almost identical. For poor quality data, no appreciable improvement is found between results from FSD and UFSD. Once again, the results from sICA have the highest correlation and the smallest error compared to the other two.

B. Phantom Data

1) Data Details: Two phantom datasets representing the realistic diffusion MR ground truth were utilized to evaluate the performance of the proposed method. The datasets are available from the open source: http://www.lnao.fr/spip.php?rubrique79. Details can be found in [45]. The phantom data were originally designed to compare the performance of fiber tractography algorithms. It simulates a coronal section of the human brain, containing several fiber crossing and kissing configurations with different curvatures. Both datasets were acquired based on 64 gradient directions. The first dataset has a b-value of 1500 $\mathrm{s/mm^2}$ and the second 2000 $\mathrm{s/mm^2}$.

A region of interest (ROI) containing crossing fibers is selected and shown as the white box in Fig. 7(e). Four methods, AQBI, UFSD, FSD, and sICA, were applied. The AQBI method [31] simplifies the process of dODF reconstruction by introducing SHT to the original QBI method. The dODF usually appears to be overly smooth like a "blurred version" of fODF. Compared to AQBI, sICA produces a "sharpened version" of

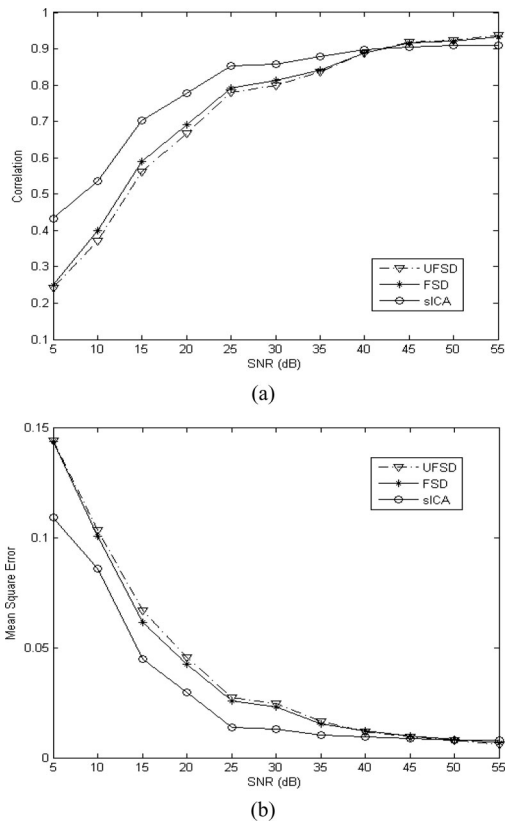

Fig. 5. Comparison of the performance under various SNRs, $Ng = 25$. (a) Correlation coefficients, (b) MSE.

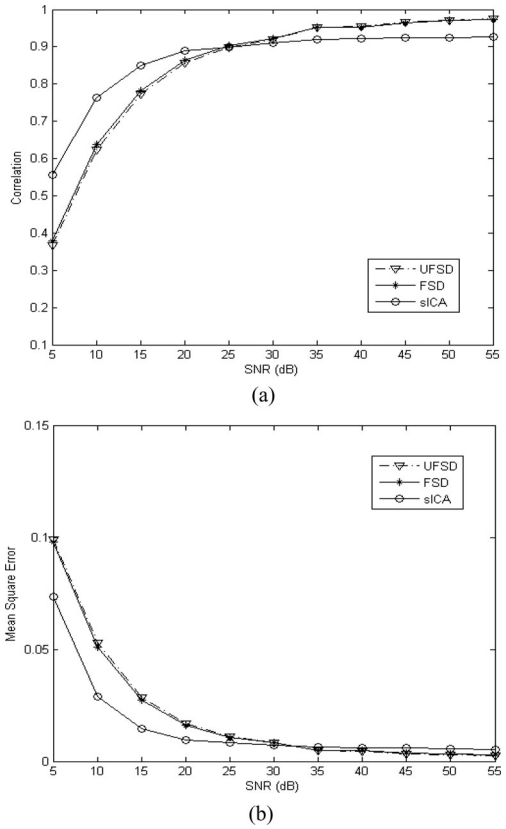

Fig. 6. Comparison of the performance under various SNRs, $Ng = 55$. (a) Correlation coefficients, (b) MSE.

fODF. (To clarify, the term ODF is used to refer to dODF and fODF in the following part.) For AQBI, an SH order of 8 with a Laplace-Beltrami regulation factor 0.006 was used [31]. The parameter settings in UFSD, FSD, and sICA were the same as in the numerical simulations. To improve the visualization results, the reconstructed ODFs were overlaid over the phantom data B0 image (the DWI with no magnetic gradient filed applied), and the voxels outside crossing fibers were excluded in the visualization. For *in vivo* data, ODFs are usually overlaid over FA maps. Here, this is unnecessary because the ground truth of fibers is clearly visible in the B0 image.

2) Results: The results from two datasets are given in Figs. 7 and 8. For both datasets, it is observed that multiple peaks are reconstructed in the fiber crossing area, which agree with the known ground truth. As expected, the AQBI results in ODFs smoother than UFSD and FSD, and the results from FSD appear to be less sharp than UFSD due to the smoothing effect of filtering. By extracting the desired ODF from the initial estimation from UFSD, sICA clearly has more sharply defined peaks than AQBI, UFSD, and FSD.

It is also noticed that the results of UFSD from the first dataset [Fig. 7(g)] appear to have better defined peaks than those from the second dataset [Fig. 8(f)]. This is because increasing the b-value also increases the noise level in the second dataset. Without filtering, the ODFs turn out to be relatively noisy. After filtering, the effect of noise is slightly reduced, but filtering also partially reduces the angular resolution of ODFs as shown in Fig. 8(g). These results are in accordance with the simulation. To demonstrate the effect of filtering, an additional example is given in Fig. 8(h). By changing the attenuation factor to $\beta = [1, 1, 0.4]$, it can be seen that the ODFs become smoother than those in Fig. 8(g).

C. In Vivo Data

1) Data Details: The *in vivo* DWI data were acquired by a 3T Signa scanner (GE Medical Systems, Milwauke, WI) from a healthy subject. A b-value of $1000\,\mathrm{s/mm^2}$ and 55 gradient directions were used as in typical DT model based clinical studies. Each volume contains 25 slices, each with dimension 256×256, field of view (FOV) 24 cm, voxel size $0.973 \times 0.973 \times 3\,\mathrm{mm}^3$, echo time (TE) 87 ms and repetition time (TR) 10000 ms. Fig. 9 shows DWI images taken from the same slice. Fig. 9(a) shows the B0 image, the DWI data collected without magnetic gradient applied. Fig. 9(b) gives a DWI image based on one gradient direction. Fig. 9(c) is the FA map obtained by using Slicer 3-D software [44]. It can be seen that the FA map provides more details about inner fiber structure than the raw DWI image.

2) Results: For *in vivo* data, the ground truth of the fiber structure is not clearly known as in the phantom data, but there are some regions in the brain which have been previously studied by other researchers. For this dataset, an ROI in a coronal section of the brain was selected according to [30], in which a similar region was used to evaluate the performance of the AQBI method. The ROI is shown as the white box on a coronal view of the FA map overlaid in Fig. 10(a).

The results from AQBI, UFSD, FSD, and sICA are given in Fig. 10 alongside the magnified view of ODFs for the selected voxels in the areas containing multiple fiber populations. In each voxel, the estimated ODFs are directionally colour-coded and superimposed over the corresponding FA map. From Fig. 10, the main contributing fiber tracts can be identified which are consistent with known anatomy. For example, the commissural fibers connecting the left and right hemispheres are shown in red. The projection tracts connecting the cerebral cortex with subcortical structures are oriented superoinferiorly, which are shown in blue. The superior longitudinal fasciculus connecting the regions from front to back within a hemisphere are shown in green.

In the areas containing multiple fiber bundles (white box in Fig. 10), it can be seen from the enlarged view of the selected voxels that the ODFs from UFSD, FSD, and sICA are much sharper than those from AQBI. Again as expected, the results from FSD are slightly smoother than those from UFSD, and the sICA improves the performance by providing more clearly defined peaks than both UFSD and FSD. These results agree with results from both numerical simulations and phantom data.

V. Discussion

In this paper, we have introduced a novel framework to enhance the fODF reconstruction in DWI, in which a single channel ICA is incorporated with the SD-based reconstruction method. Results from numerical simulations, phantom data and

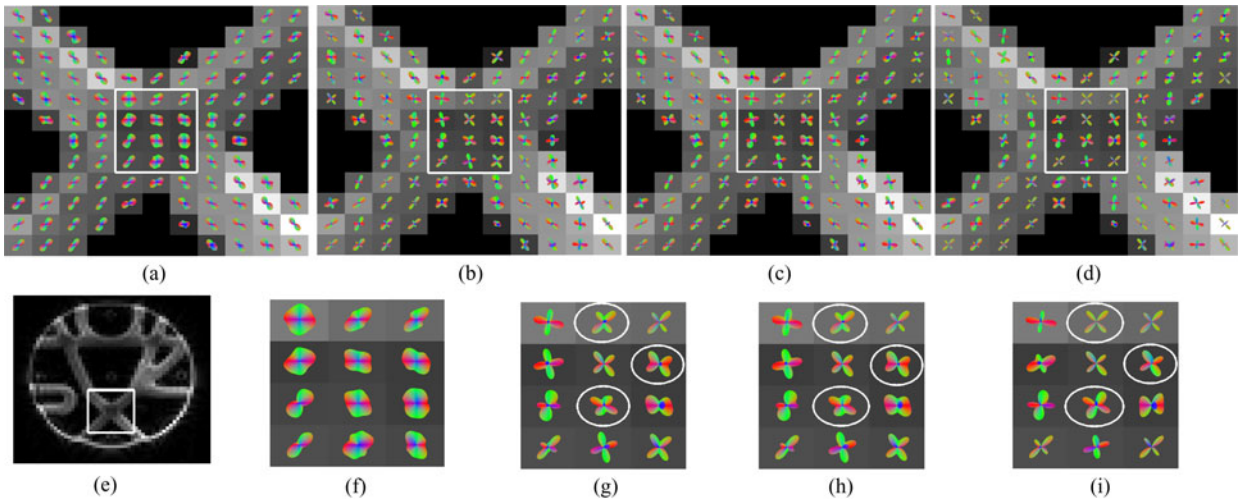

Fig. 7. Results from the first phantom dataset (b-value of 1500 $\mathrm{s/mm^2}$): (a) AQBI, (b) UFSD, (c) FSD, and (d) sICA. The enlarged view of ODFs from four methods in the selected voxels are given in (f), (g), (h), and (i), respectively. The phantom data are shown in (e), in which the white box indicates the ROI.

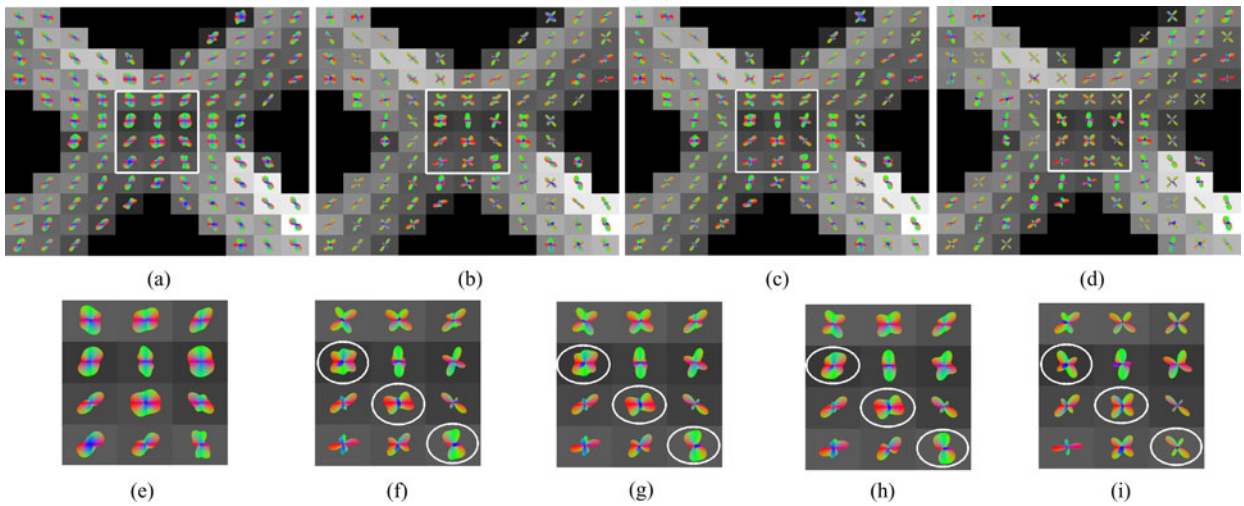

Fig. 8. Results from the second phantom dataset (b-value of 2000 $\mathrm{s/mm^2}$): (a) AQBI, (b) UFSD, (c) FSD, and (d) sICA. The enlarged view of ODFs from four methods in the selected voxels are given in (e), (f), (g), and (i), respectively. To demonstrate the effect of filtering, an additional example from FSD is given in (h) by increasing the attenuation level of filtering.

in vivo data have demonstrated that the proposed method not only improves the angular resolution of fODFs, but also enhances the robustness to noise and variation in b-values. Though this study was focused on enhancement of fODF reconstruction in low angular resolution DWI, the proposed framework can be applied to any HARDI-based study. By decomposition, we can obtain rich information about the components of ODFs and, therefore, help to gain a deeper understanding about inner fiber reconstruction and the relationship between ODF components.

We also explored the potential of applying the proposed method to DWI data acquired with relatively low b-value (1000 $\mathrm{s/mm^2}$), which is commonly used in clinical studies. The HARDI-based methods require high angular resolution and high b-values, which are not suitable for such data without additional improvements in methodology. The promising results of sICA from this study suggest that the proposed method has the potential to improve the qualitative description of inner fiber architecture if applied to low angular resolution DWI data from human brain white matter studies.

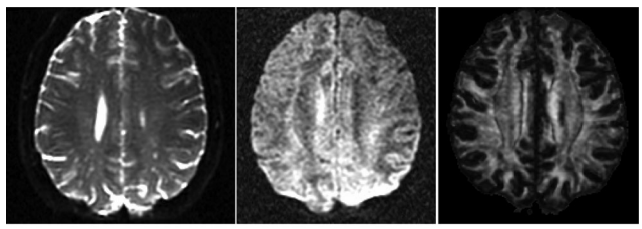

Fig. 9. *In vivo* DWI images taken from the same slice. (a) B0 image, (b) DWI image, and (c) FA map.

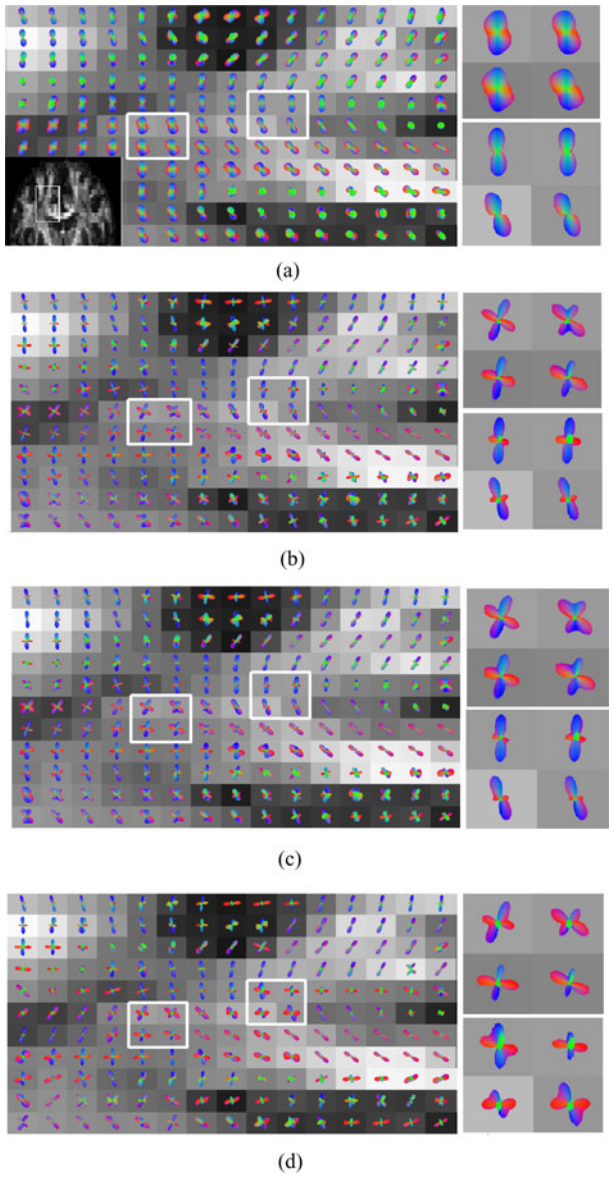

Fig. 10. Results of ODFs obtained from *in vivo* data (b = 1000 $\mathrm{s/mm^2}$, 55 directions) with enlarged views of ODFs from selected voxels: (a) AQBI, (b) UFSD, (c) FSD, and (d) sICA.

The presence of negative values in results of fODFs is one common issue in deconvolution-based methods. In this work, due to fewer gradient directions in the data acquisition, only SH order of 4 was used and the effect of the negative values was relatively small. Those negative values can therefore be ignored as in [12], [15]. Deconvolution-based methods have a problem in isotropic regions, which has not been tackled in this study, as the proposed method is based on fODF initially estimated from the SD method. One solution for this was applied in [28], in which the FA value was used as the threshold to exclude those isotropic voxels, so the proposed method can be mainly applied to the anisotropic voxels.

It is noticed that the process in the sICA model has some similarity with singular-spectrum analysis (SSA) [41]. The SSA decomposes the time series into several additive components, such as the slowly varying parts of a time series, various "oscillatory" components and noise components. But SSA usually applies singular value decomposition (SVD) or principal component analysis (PCA), so the components are orthogonal but not necessarily statistically independent as in sICA.

Like all ICA approaches, the proposed method faces open issues such as ambiguities in scaling and order of outputs, selection of the number of components and identification of desired components. The scaling ambiguity was solved by prewhitening so that all ICs were normalized. Generally, the number of components can be estimated based on a threshold for eigenvalues and the desired IC can be selected based on prior knowledge, but this is not suitable here as there is still no proper method to identify the desired IC from the outputs in this study. In [37], [39], a grouping process was carried out to classify the spectrum of ICs based on k-means clustering; the desired component was then selected based on the prior knowledge. In [38], the desired IC was selected by visual inspection. These approaches are not applicable here due to lack of prior information about the true fODF in real data. In this study, we set the number of IC as 2, because we wished to obtain only two ICs (fODF and noise), and the IC with a greater energy (the most dominant component) was selected from the two ICs. These parameter settings appear to work well in both phantom and *in vivo* data. The results from the phantom data agree with the ground truth, and the results from the *in vivo* data appear to be in accordance with the known contributing fiber tracts.

However, it should be noted that the parameter settings in this sICA application were based on the fact that we were working on the DWI with a relatively small number of directions, so an SH of order-4 was used. It has been noticed in our study that with an increase of SH order, the ICs from sICA become complex and 2 ICs are no longer suitable. Further investigation is needed to find out more information about the desired fODF. If such prior information is available, the number of ICs can be estimated accordingly and the selection of desired components can be achieved by a proper postprocessing approach or by adding a constraint into the separation process.

VI. Conclusion

In this paper, we have presented a novel framework in which the well known ICA technique is incorporated with a spherical deconvolutionbased method to enhance the performance of fODF reconstruction in low angular resolution DWI. In the present study, a single channel ICA model was employed to decompose an initial estimation of fODF by the SD method, which is considered as a signal mixed with noise, artifacts and desired "true" fODF. The results from numerical simulations, phantom data and in vivo data demonstrate that sICA can separate the fODF from the noise and artifacts, which not only achieves better performance in terms of robustness to noise and variations in b-values, but also improves the angular resolution of fODF in fiber crossing areas. The proposed new framework provides a link by which advanced fiber orientation reconstruction methods can be applied to clinical studies. Apart from these, with future improvements to the algorithm, the proposed framework

can also be considered as a general enhancement technique for DWI research.

ACKNOWLEDGMENT

The authors thank the anonymous reviewers for valuable comments to improve the scientific quality of the paper. The authors also thank Dr. Maxime Descoteaux of Sherbrooke University, Canada, for providing the original MATLAB code for the AQBI and SD simulation, Dr. Slava Murzin from the Center for the Complex Systems and Brain Sciences at Florida Atlantic University for helping to collect DWI data, and Dr. David Watson from the Intelligent Systems Research Centre, University of Ulster, Coleraine, Nortern Ireland, for valuable advices and discussions.

REFERENCES

[1] P. J. Basser, J. Mattiello, and D. Le Bihan, "MR diffusion tensor spectroscopy and imaging," *Biophys. J.*, vol. 66, pp. 259–267, 1994.

[2] P. J. Basser, J. Mattiello, and D. Le Bihan, "Estimation of the effective self-diffusion tensor from the NMR spin echo," *J. Magn. Reson.*, vol. 103, pp. 247–254, 1994.

[3] M. J. Hoptman, F. M. Gunning-Dion, C. F. Murphy, B. A. Ardekani, J. Hrabe, K. O. Lim, G. R. Etwaroo, D. Kanellopoulos, and G. S. Alexopoulos, "Blood pressure and white matter integrity in geriatric depression," *J. Affective Disorders*, vol. 115, pp. 171–176, 2009.

[4] D. R. Rutgers, P. Fillard, G. Paradot, M. Tadie, P. Lasjaunias, and D. Ducreu, "Diffusion tensor imaging characteristics of the corpus callosum in mild, moderate, and severe traumatic brain injury," *Amer. J. Neuroradiol.*, vol. 29, no. 9, pp. 1730–1735, 2008.

[5] A. Fuchs, K. J. Jantzen, and J. A. S. Kelso, "Diffusion tensor imaging analysis of sequential scans in mild traumatic brain injuries," in *Proc. 38th Annu. Meet. Soc. Neurosci.*, Washington, DC, Nov. 15–19, 2008.

[6] N. H. Stricker, B. C. Schweinsburg, L. Delano-Wood, C. E. Wierenga, K. J. Bangen, K. Y. Haaland, L. R. Frank, D. P. Salmon, and M. W. Bondi, "Decreased white matter integrity in late-myelinating fiber pathways in Alzheimer's disease supports retrogenesis," *NeuroImage*, vol. 45, pp. 10–16, 2009.

[7] D. S. Tuch, T. G. Reese, M. R. Wiegell, N. Makris, J. W. Belliveau, and V. J. Wedeen, "High angular resolution diffusion imaging reveals intravoxel white matter fiber heterogeneity," *Magn. Reson. Med.*, vol. 48, pp. 577–582, 2002.

[8] D. S. Tuch, "Q-ball imaging," *Magn. Reson. Med.*, vol. 52, pp. 1358–1372, 2004.

[9] V. Wedeen, T. Reese, D. Tuch, M. Wiegel, J. G. Dou, R. Weiskoff, and D. Chessler, "Mapping fiber orientation spectra in cerebral white matter with fourier-transform diffusion MRI," *Proc. Int. Soc. Magn. Reson. Med.*, vol. 8, p. 82, 2000.

[10] K. M. Jansons and D. C. Alexander, "Persistent angular structure: New insights from diffusion magnetic resonance imaging data," *Inverse Problems*, vol. 19, pp. 1031–1046, 2003.

[11] E. Ozarslan, T. Shepherd, B. Vemuri, S. Blackband, and T. Mareci, "Resolution of complex tissue microarchitecture using the diffusion orientation transform (DOT)," *NeuroImage*, vol. 31, no. 3, pp. 1086–1103, 2006.

[12] J. Tournier, F. Calamante, D. G. Gadian, and A. Connelly, "Direct estimation of the fiber orientation density function from diffusion-weighted MRI data using spherical deconvolution," *Neuroimage*, vol. 23, pp. 1176–1185, 2004.

[13] H. E. Assemlal, D. Tschumperlé, L. Brun, and K. Siddiqi, "Recent advances in diffusion MRI modeling: Angular and radial reconstruction," *Med. Image Anal.*, vol. 15, no. 4, pp. 369–396, 2011.

[14] C. Lenglet, J. S. W. Campbell, M. Descoteaux, G. Haro, P. Savadjiev, D. Wassermann, A. Anwander, R. Deriche, G. B. Pike, G. Sapiro, K. Siddiqi, and P. M. Thompson, "Mathematical methods for diffusion MRI processing," *NeuroImage*, vol. 45, pp. 111–122, 2009.

[15] M. Descoteaux, R. Deriche, T. R. Knsche, and A. Anwande, "Deterministic and probabilistic tractography based on complex fibre orientation distributions," *IEEE Trans. Med. Imag.*, vol. 28, no. 2, pp. 269–286, Feb. 2009.

[16] S. Sanei and J. Chambers, *EEG Signal Processing*. New York: John Wiley & Sons, 2007.

[17] M. Jing and S. Sanei, "Simultaneous EEG-fMRI analysis with application to detection of seizure signal sources," *Recent Advances in Signal Processing*, Cape Tpwn, SA: InTech Publishing, pp. 441–458, 2009.

[18] K. Arfanakis, D. Cordes, V. M. Haughton, J. D. Carew, and M. E. Meyerand, "Independent component analysis applied to diffusion tensor MRI," *Mag. Reson. Med.*, vol. 47, pp. 354–363, 2002.

[19] A. R. Franco, J. Ling, A. Caprihan, V. D. Calhoun, R. E. Jung, G. L. Heileman, and A. R. Mayer, "Multimodal and multi-tissue measures of connectivity revealed by joint independent component analysis," *IEEE J. Sel. Top. Signal Process.*, vol. 2, no. 6, pp. 986–997, Dec. 2008.

[20] S. Kim, J. Jeong, and M. Singh, "Estimation of multiple fiber orientations from diffusion tensor MRI using independent component analysis," *IEEE Trans. Nuclear Sci.*, vol. 52, no. 1, pp. 266–273, Feb. 2005.

[21] J. O'Muircheartaigh, C. Vollmar, C. Traynor, G. J. Barker, V. Kumari, M. R. Symms, P. Thompson, J. S. Duncan, M. J. Koepp, and M. P. Richardsona, "Clustering probabilistic tractograms using independent component analysis applied to the thalamus," *Neuroimage*, vol. 54, no. 3, pp. 2020–2032, 2011.

[22] D. M. Healy, H. Hendriks, and P. T. Kim, "Spherical deconvolution," *J. Multivar. Anal.*, vol. 67, pp. 1–22, 1998.

[23] D. C. Alexander, "Maximum entropy spherical deconvolution for diffusion MRI," *Image Process. Med. Imag.*, pp. 76–87, 2005.

[24] J. Tournier, F. Calamante, and A. Connelly, "Robust determination of the fibre orientation distribution in diffusion MRI: Non-negativity constrained super-resolved spherical deconvolution," *NeuroImage*, vol. 35, pp. 1459–1472, 2007.

[25] A. Anderson, "Measurements of fiber orientation distributions using high angular resolution diffusion imaging," *Magn. Reson. Med.*, vol. 54, pp. 1194–1206, 2005.

[26] T. E. J. Behrens, M. W. Woolrich, M. Jenkinson, H. Johansen-Berg, R. G. Nunes, S. Clare, P. M. Matthews, J. M. Brady, and S. M. Smith, "Characterization and propagation of uncertainty in diffusion-weighted MR imaging," *Magn. Reson. Med.*, vol. 50, pp. 1077–1088, 2003.

[27] B. Jian and B. C. Vemuri, "Unifed computational framework for deconvolution to reconstruct multiple fibers from diffusion weighted MRI," *IEEE Trans. Med. Imag.*, vol. 26, no. 11, pp. 1464–1471, Nov. 2007.

[28] F. DellAcqua, G. Rizzo, P. Scifo, R. Clarke, G. Scotti, and F. Fazio, "A model-based deconvolution approach to solve fiber crossing in diffusion-weighted MR imaging," *IEEE Trans. Biomed. Eng.*, vol. 54, no. 3, pp. 462–472, Mar. 2007.

[29] M. Jing, T. M. McGinnity, S. Coleman, and H. Zhang, "Incorporating ICA to Q-ball imaging for diffusion orientation distribution reconstruction," in *Proc. 32nd IEEE Eng. Med. Biol. Conf. (EMBC)*, Sep. 2010, pp. 2706–2709.

[30] C. P. Hess, P. Mukherjee, E. T. Han, D. Xu, and D. B. Vigneron, "Q-ball reconstruction of multimodal fiber orientations using the spherical harmonic basis," *Magn. Reson. Med.*, vol. 56, no. 1, pp. 104–117, 2006.

[31] M. Descoteaux, E. Angelino, S. Fitzgibbons, and R. Deriche, "Regularized, fast, and robust analytical q-ball imaging," *Magn. Reson. Med.*, vol. 58, no. 3, pp. 497–510, 2007.

[32] M. Descoteaux, E. Angelino, S. Fitzgibbons, and R. Deriche, "Apparent diffusion coefficients from high angular resolution diffusion imaging: Estimation and applications," *Magn. Reson. Med.*, vol. 56, pp. 395–410, 2006.

[33] A. J. Bell and T. J. Sejnowski, "An information-maximization approach to blind separation and blind deconvolution," *Neural Comput.*, vol. 7, pp. 1129–1159, 1995.

[34] B. A. Olshausena and D. J. Field, "Emergence of simple-cell receptive-filed properties by learning a sparse code of natural images," *Nature*, vol. 381, pp. 607–609, 1996.

[35] M. Zibulevsky and B. A. Pearlmutter, "Blind source separation by sparse decomposition," *Neural Comput.*, vol. 13, no. 4, pp. 863–882, 2001.

[36] G. J. Jang and T. W. Le, "A maximum likelihood approach to single-channel source separation," *J. Mach, Learn. Res.*, vol. 4, pp. 1365–1392, 2003.

[37] M. E. Davies and C. J. James, "Source separation using single channel ICA," *Signal Process.*, vol. 87, pp. 1819–1832, 2007.

[38] B. Mijovi, M. De Vos, I. Gligorijevi, J. Taelman, and S. Van Huffel, "Source separation from single-channel recordings by combining empirical-mode decomposition and independent component analysis," *IEEE Trans. Biomed. Eng.*, vol. 57, no. 9, pp. 2188–2196, Sep. 2010.

[39] A. Jimenez-Gonzalez and C. J. James, "Extracting sources from noisy abdominal phonograms: A single-channel blind source separation method," *Med. Biol. Eng. Comput.*, vol. 47, pp. 655–664, 2009.

[40] A. Hyvärinen, J. Karhunen, and E. Oja, *Independent Component Analysis*. New York: Wiley, 2001.
[41] N. Golyandina, V. Nekrutkin, and A. Zhigljavsky, *Analysis of Time Series Structure—SSA and Related Techniques*. London, U.K.: Chapman & Hall/CRC, 2001.
[42] D. R. Salgado and F. J. Alonso, "Tool wear detection in turning operations using singular spectrum analysis," *J. Mater. Process. Technol.*, vol. 171, pp. 451–458, 2006.
[43] H. Gudbjartsson and S. Patz, "The Rician distribution of noisy MRI data," *Magn. Reson. Med.*, vol. 34, pp. 910–914, 1995.
[44] S. Pieper, M. Halle, and R. Kikinis, "3-D SLICER," in *Proc. 1st IEEE Int. Symp. Biomed. Imag.: Nano Macro*, 2004, vol. 1, pp. 632–635.
[45] P. Fillard, M. Descoteaux, A. Goh, S. Gouttard, B. Jeurissen, J. Malcolmg, A. Ramirez-Manzanares, M. Reisert, K. Sakaie, F. Tensaouti, T. Yo, J. F. Mangin, and C. Pouponm, "Quantitative evaluation of 10 tractography algorithms on a realistic diffusion MR phantom," *NeuroImage*, vol. 56, pp. 220–234, 2011.

Min Jing received the M.Sc. degree in digital signal processing (with distinction) from King's College, London, UK, in 2004, and the Ph.D. degree in biomedical signal processing from the Centre of Digital Signal Processing, Cardiff University, Wales, UK, in 2008. Her doctoral research was focused on the investigation of predictability of epileptic seizure by fusion of EEG and fMRI.

She is currently a Research Associate in the Computational Neuroscience Research Team, Intelligent Systems Research Centre, University of Ulster, Coleraine, Nortern Ireland. Her current research interests are focussed on the development and implementation of advanced signal processing techniques in diffusion tensor imaging and fMRI, with application to brain white matter related diseases and neurodegeneration.

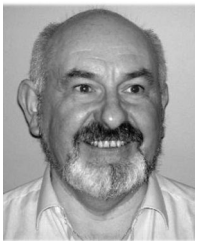

T. Martin McGinnity (M'83–SM'09) received the First Class (Hons.) degree in physics, and a Ph.D. degree from the University of Durham, Durham, UK.

He is a Professor of Intelligent Systems Engineering with the Faculty of Computing and Engineering, University of Ulster, Coleraine, Nortern Ireland. He is currently Director of the Intelligent Systems Research Centre, which encompasses the research activities of approximately 100 researchers. Formerly, he was Associate Dean of the Faculty and Director of both the University's technology transfer company, Innovation Ulster, and a spin out company Flex Language Services. He is the author or coauthor of more than 250 research papers. His current research interests are focussed on the creation of bio-inspired intelligent computational systems which explore and model biological signal processing, particularly in relation to cognitive robotics, and computation neuroscience modeling of neurodegeneration. He has been awarded both a Senior Distinguished Research Fellowship and a Distinguished Learning Support Fellowship in recognition of his contribution to teaching and research.

Prof. McGinnity is a Fellow of the IET and a Chartered Engineer.

Sonya Coleman (M'11) received the B.Sc.(Hons.) degree in mathematics, statistics, and computing, in 1999, and the Ph.D. degree in mathematics, in 2003, all from the University of Ulster, Coleraine, Nortern Ireland.

She is currently a lecturer in the School of Computing and Intelligent System at the University of Ulster, Magee. She has more than 60 publications primarily in the field of mathematical image processing. In 2009, she was awarded the Distinguished Research Fellowship by the University of Ulster in recognition of her contribution in research.

Huaizhong Zhang (M'09) received the B.Sc. and M.Sc. degrees, in mathematics and applied mathematics, in 1984 and 1990, respectively, and the M.Eng. and Ph.D. degrees in computer science from the University of Ulster, Nortern Ireland, U.K., in 1997 and 2010, respectively.

He is a Research Associate in the Intelligent Systems Research Centre (ISRC), University of Ulster, Coleraine, Nortern Ireland. His main research interests lie in biomedical image processing, machine learning, and data analysis, with a particular emphasis on the applications of Bayesian and variational methods in biomedical image processing, and diffusion-weighted MRI.

Armin Fuchs was born in Nürtingen, Germany, in 1959. He received a diploma, in 1985, and the Ph.D. degree in theoretical physics from the University of Stuttgart, Germany, in 1990.

He is currently an Associate Professor of physics and complex systems and brain sciences at Florida Atlantic University in Boca Raton, Florida. His research interests include data analysis for noninvasive brain imaging methods and modeling using nonlinear dynamical systems.

J. A. Scott Kelso was born in Derry, Northern Ireland. He received the undergraduate degree from The University of Calgary in 1972, and the M.Sc. and the Ph.D. degrees, in 1973 and 1975, respectively, from the University of Wisconsin, Madison, WI, where he studied neural mechanisms underlying the coordination and control of movement. He was educated at Foyle College, Londonderry, U.K., and trained originally as a teacher at Stranmillis University College, Belfast, U.K., graduating with honors, in 1969.

From 1976 to 1978, he was an Assistant Professor and Director of the Motor Behavior Laboratory at the University of Iowa. Between 1978 and 1985, he was a Senior Research Scientist at Haskins Laboratories, Yale University, Associate Professor (1978) and Professor (1982) of psychology and biobehavioral sciences at the University of Connecticut (unit of behavioral genetics). Since 1985, he is Glenwood and Martha Creech Eminent Scholar Chair in Science at Florida Atlantic University, where he founded and directed the first Center for Complex Systems and Brain Sciences in the US. For more than 20 years he led an NIH-funded National Training Program in this new interdisciplinary field. In 2009, Kelso was appointed Visiting Professor of computational neuroscience at the Intelligent Systems Research Centre at The University of Ulster Magee Campus in Derry, where he helps guide a small team of researchers. He has been a Guest Professor with Lyons (1983), Stuttgart (1984), Moscow (1986), Marseille (2000), and Belo Horizonte, Brasil (2011) and was a Fellow of The Neurosciences Research Institute in La Jolla, CA (1997). He is the author of more than 300 research papers in disciplines like neuroscience, psychology, physiology, biology, and physics. His books include *Dynamic Patterns: The Self-Organization of Brain and Behavior* (1995/1997, MIT Press), *Coordination Dynamics* (with V. K. Jirsa, Springer, 2004), and *The Complementary Nature* (with D.A. Engstrøm, MIT Press, 2006/2008). For most of his scientific career he has used a combination of brain imaging, behavioral methods, and theoretical modeling to understand how human beings (and human brains)—individually and together—coordinate behavior at multiple levels, from the cellular to the social. He is considered a pioneer in the field of coordination dynamics, a theoretical and empirical framework geared to uncovering the principles and mechanisms of functional coordination in living things. A recent invited piece "Coordination Dynamics" is published by Springer in their Encyclopedia of Complexity and System Science (2009).

Prof. Kelso is a fellow of AAAS, APA, and APS. He is the recipient of numerous awards including the MERIT, Senior Scientist, and Director's Innovation Awards from NIH, the Distinguished Alumni Research Achievement Award from the University of Wisconsin, Madison, and the Docteur Honoris Causa degrees from the Republic of France and the University of Toulouse. In December 2007, he was honored to be named Pierre de Fermat Laureate, and in 2011 he received the Bernstein Prize from the International Society of Motor Control.